Conf-740827--1

EFFECTS OF PROTON BOMBARDMENT ON SELF-DIFFUSION IN SILVER: A PRELIMINARY REPORT

by

Nghi Q. Lam, S. J. Rothman, K. L. Merkle,
L. J. Nowicki, and D. J. Dever

For Presentation at:

International Conference on Low Temperature Diffusion,
Thomas J. Watson Research Center, Yorktown Heights, New York,
August 12-14, 1974

U of C-AUA-USAEC

ARGONNE NATIONAL LABORATORY, ARGONNE, ILLINOIS

EFFECTS OF PROTON BOMBARDMENT ON SELF-DIFFUSION IN SILVER: A PRELIMINARY REPORT*

Nghi Q. Lam, S. J. Rothman, K. L. Merkle, L. J. Nowicki, and D. J. Dever

Argonne National Laboratory
Argonne, Illinois 60439

The radiation-enhanced self-diffusion coefficient (D_{rad}) in silver under 270-keV proton bombardment has been measured over the temperature range from 240 to -60°C. The flux dependence of D_{rad} has also been studied at 106 and 179°C with the flux varying from 2.5×10^{12} to 6.3×10^{13} protons/cm^2-sec. The experimental data are analyzed in the framework of the classical model involving single vacancies and interstitials as mobile defects.

*Work performed under the auspices of the U.S. Atomic Energy Commission.

1. INTRODUCTION

Mass transport by means of point defects introduced by irradiation is connected with technologically important phenomena such as swelling in fast reactor cladding,[1] diffusion during ion implantation,[2] and defect-cluster formation in the high-voltage electron microscope.[3,4] In addition, such mass transport is of fundamental interest from the viewpoint of the behavior of point defects. The kinetics of mass transport under irradiation, or radiation-enhanced diffusion, have been studied[4-9] on the basis of the following model:

1) vacancies and interstitials are created in equal numbers by the irradiation at a rate of J atomic fraction/sec;

2) the vacancies and interstitials diffuse by random walk with the same diffusion coefficients D_v and D_i, respectively, as in the absence of irradiation;

3) The radiation-enhanced-diffusion coefficient is given by $D_{rad} = D_v C_v + D_i C_i$, where C_v and C_i are the atom fractions of vacancies and interstitials, respectively ($D_i >> D_v$);

4) the vacancies and interstitials are annihilated by mutual recombination or at fixed sinks (sink concentration = C_s). The rate constants for these processes are

$K_{iv} = 4\pi r_{iv} (D_i + D_v)/\Omega$ [10] for mutual recombination,

$K_{sv} = 4\pi r_{sv} D_v/\Omega$ and

$K_{si} = 4\pi r_{si} D_i/\Omega$ for the annihilation of vacancies or interstitials, respectively, at fixed sinks. The quantities r_{iv}, r_{sv}, and r_{si} are the capture radii of the vacancy for an interstitial, of a sink for a vacancy or interstitial, respectively, and Ω is the atomic volume.

If the temperature is sufficiently high so that a steady-state point-defect concentration is attained in a shorter time than the duration of the experiment, the vacancies and interstitials contribute equally to the mass transport, and

$$D_{rad} = 2 JD_i/K_{si}C_s \tag{1}$$

for predominant annealing to fixed sinks (AFS),[4,9] or

$$D_{rad} = 2 (J D_i D_v/K_{iv})^{1/2} \tag{2}$$

for predominant mutual recombination (MR).[4,9] (There will, of course, be an intermediate region where the two effects are equal). Thus, at high temperatures and/or high sink densities, where AFS is favored, D_{rad} should vary linearly with the defect production rate and should be independent of temperature. At lower temperatures, lower sink densities, and/or high defect production rates, where MR is favored, D_{rad} should increase as the square root of the defect production rate and vary with temperature according to an Arrhenius law with the activation energy equal to $H_v^m/2$, half the vacancy motion energy. At still lower temperatures or quite low sink densities, steady state is not reached and one expects dominant interstitial transport.[11] The flux dependence in this regime is always $\sqrt{J}$ (it is assumed that the defect production rate is linearly proportional to the flux), but the activation energy can vary from zero to one-half of the interstitial motion energy ($H_i^m/2$, depending on the details of the defect buildup.[6]

In addition to the theoretical work outlined here, a large number of experimental studies of diffusion under irradiation have been made.[11-18] In most of these studies, D_{rad} was obtained from indirect measurements such as ordering. Although such experiments have confirmed some aspects of the above model, it was thought desirable to carry out a complete investigation by means of a classical technique that would most directly reflect the behavior of the point defects. For this reason, we chose to measure self-diffusion in silver by the thin-layer sectioning technique.[19-20]

Unfortunately, this technique introduces a complication in that the surface on which the thin layer of radiotracer is deposited acts as a sink for point defects. That is, at $x = 0$ the radiation-induced defect concentration and therefore D_{rad} are equal to zero. The defect concentration increases linearly[15,21] with distance x from the surface ($D_{rad} = D_x x$) to a distance greater than the thickness of the diffusion zone at $T > 80°C$. The spatial distribution of the concentration of the radioisotope after diffusion at $T > 80°C$ is given by[22]

$$C = \frac{M}{D_x t} \exp\left(-\frac{x}{D_x t}\right) . \qquad (3)$$

Here M is the amount of isotope deposited, t is the time of anneal, and D_x is related to D_{rad} in the bulk (i.e., far from the surface) by[15,21]

$$D_{rad} = D_x^2/2J . \qquad (4)$$

At low temperatures, the distance over which the point-defect concentrations vary is assumed to be small, compared with the thickness of the diffusion zone.[9] We thus neglect the perturbation caused by the surface and use the classical Gaussian solution[17]

$$C = \frac{M}{(\pi D_{rad} t)^{1/2}} \exp(-x^2/4 D_{rad} t) \qquad (4a)$$

to calculate D_{rad} from the experimental data.

2. EXPERIMENTAL

2.1 Sample Preparation

The samples were cylindrical single crystals of 5N silver, with the rod axis parallel to a high index direction to avoid channeling. One end of the crystal was gound, polished, and chemically polished.[19] The crystal was subsequently annealed at 955°C. The flat end was chemically repolished, anodized, and stripped a few times, and electroplated with a thin ($\sim$ 10°A) layer of ^{110m}Ag.

2.2 Irradiation

The plated face of the crystal was irradiated with a defocused beam of 270-keV protons at a direction normal to the crystal surface. The fluxes varied from 2.5×10^{12} to 6.25×10^{13} protons/cm^2-sec; the majority of the experiments was conducted at 1.25×10^{13} protons/cm^2-sec. The beam was swept at a frequency of 1 KHz to obtain a uniform irradiation over the entire bombarded area. Irradiation times ranged from 2.8×10^3 to 4.32×10^4 sec. The irradiation was carried out in a vacuum of 10^{-7} Torr.

The sample temperature was controlled to ± 0.5°C between -60 and 240°C by circulating alcohol or high-temperature oil through a copper tube welded to the large copper cylinder in which the sample was held. The sample temperature was measured with a thermocouple that was inserted into a radial hole ∿ 3 mm below the bombarded surface.

2.3 Diffusion Measurements

The cylindrical sides of the sample and the edge of the irradiated surface were masked with Tygon paint, and the sample was sectioned by the anodizing-stripping technique.[19] The section thickness, predicted from the previously obtained calibration was determined to ± 10% by weighing the sample before and after sectioning. The stripping solutions were radioassayed by scintillation counting.

3. RESULTS

3.1 Penetration Plots

The penetration plots, log C vs x/t, are linear for high temperatures, as expected from eqn. (3) (Fig. 1). The deviations from linearity at the low activity ends of the penetration plots are thought to be due to imperfect surface preparation.[20] The penetration plots for low temperatures are linear when plotted as log C vs x^2 [eqn. (4a)], with some upward deviation near the surface (Fig. 2). Several blanks were run, and their penetration plots were completely different from those in Fig. 1; thus a real radiation effect exists. The values of D_x or D_{rad} obtained from the penetration plots are given in Tables I-III.

3.2 Values of D_{rad}

The values of the bulk radiation-enhanced-diffusion coefficient, D_{rad}, are also given in Tables I-III. These tables refer to three series of experiments: constant flux, varying temperature (Table I); varying flux, constant temperature of 106°C (Table II); and varying flux, constant temperature of 179°C (Table III). The values of D_{rad} are plotted versus temperature (1st series) in Fig. 3 and versus flux (2nd and 3rd series) in Figs. 4 and 5. Figure 3 also shows the values of the thermally activated diffusion coefficient[20] (without irradiation) and the values of D_{rad} calculated from eqn. (2) for steady state and dominant MR. In addition, the low-temperature, nonsteady state values of D_{rad}, calculated from[6]

$$D_{rad} = D_i \, [J/2 \, K_{iv} \, K_{si} \, C_s]^{1/2} \, t^{-1/2} \, , \qquad (5)$$

are shown in Fig. 3. Figures 4 and 5 show that D_{rad} varies as the square root of the flux (the exponent of the flux is 0.47 ± 0.05 at 179°C and 0.6 ± 0.2 at 106°C).

4. DISCUSSION

4.1 Comparison of Theory with Experiment

The main objective of the present work is to compare the measured D_{rad} with that obtained from the theory described in eqns. (1) or (2) of the Introduction. To make such a comparison, we must know the quantities that comprise the right-hand side of eqn. (1) or (2), the defect-production rate J, the vacancy diffusion coefficient D_v, the sink density C_s, and the capture radii, r_{iv} and r_{si}. The defect-production rate is a calculated

quantity that is not known to better than a factor of three (see below). D_v is obtained by extrapolation from high-temperature data[23] and is uncertain by perhaps a factor of ten. Our estimate of the overall sink density C_s, including radiation-induced sinks, is also uncertain by a factor of ten. This quantity can be roughly measured by transmission electron microscopy, and we are now beginning such measurements; the present report must therefore be considered preliminary. In any case, it is evident that quantitative agreement between theory and experiment means agreement within these quite large uncertainties; however, it is possible to compare the experimental and theoretical variations of D_{rad} with flux or temperature.

The correct equation for D_{rad} depends on whether steady state has been attained, and if so, whether MR or AFS is dominant. As will be shown in the section on steady state below, it seems probable that steady state was attained at high temperatures ($T \gtrsim 150°C$) and not at low temperatures. Assuming that grown-in dislocations are the only sinks present, i.e., $C_s \approx 10^{-8}$, we find MR dominant. Thus at higher temperatures $D_{rad} \propto J^{1/2}$ and $D_{rad} \propto \exp(-H_v^m/2kT)$ [eqn. (2)], whereas at low temperatures $D_{rad} \propto J^{1/2}$, $D_{rad} \propto t^{-1/2}$, and D_{rad} is independent of temperature [eqn. (5)]. These two regions correspond to the lines marked "simple theory" in Fig. 3; agreement is satisfactory at $T > 180°C$ and $T < 55°C$. The experimentally observed square-root flux dependence of D_{rad} (Figs. 4 and 5) also agrees with dominant MR. We are not certain why the temperature dependence of D_{rad} decreases below 180°C; possible explanations involve nonsteady-state conditions or time-dependent sink concentrations.

4.2 Influence of the Calculated Point-defect Production Rate on D_{rad}

The damage creation rate is uniform across the diffusion zone, within about 6%, because the projected range of 270-keV protons in Ag is $\sim$ 1 μm, much greater than the width of the diffusion zone.

The defect-production rate was calculated on the basis of a simple Kinchin-Pease model, Rutherford scattering,[24] and a displacement energy of 28 eV,[25] which yielded 5.2×10^{-19} cm^2 as the cross section for Frenkel pair production. This cross section leads to the maximum values of J given in Table I. Correcting the calculated production rate for correlated recombination (a factor of two) and for the fact that the Kinchin-Pease model overestimates Frenkel pair formation via high-energy ion bombardment by a factor of $\sim$ 3 leads to the minimum estimate of J. Use of the latter value of J moves the experimental and theoretical values of D_{rad} (Table I) farther apart, but does not affect the temperature or flux dependence of D_{rad}. It can be seen from eqns. (1), (2), and (4) that the ratio of the theoretical to the experimental values of D_{rad} for high temperatures varies as $J^{3/2}$ (MR) or J^2 (AFS), i.e., sensitive to the value of J. We also point out that we have not taken the effect of temperature on J into account.

4.3 Time-dependent Sink Concentrations

The model we use assumes that the sink concentration is independent of time, and the sinks are identified as the grown-in dislocations. In this case $C_s \approx 10^{-8}$, and we should be operating in the MR regime even at the highest temperatures. However, point-defect aggregates can also act as sinks for mobile point defects, and these can arise from either the

agglomeration of moving point defects or displacement cascades due to high-energy knock-ons. We believe that the first of these is not important in our experiments because our measurements are made within 1000 Å of the surface, i.e., within the "denuded zone." The second effect can be important because displacement cascades as large as $\sim$ 100 vacancies can be caused by an energetic Ag recoil atom. We calculate a cross section of 1.5×10^{-22} cm^2 for the formation of clusters of 30 atoms or larger.

The effect of these clusters on D_{rad} will depend on their efficiency as sinks and on how they accummulate with time. If the density of clusters increases linearly with time, a large sink density will be reached ($C_s \approx 2 \times 10^{-3}$) after a dose of 4×10^{17} protons/cm^2. In this case, steady state will not be attained as the sink density is changing constantly with time. The other possibility is that the sink density saturates at a somewhat lower value in a time shorter than the duration of a run.[26] We should then have a high ($\approx 2 \times 10^{-4}$) sink density constant in time, which would put us into the AFS region. In this case, steady state would be attained at room temperature.

Another important but unknown property of these cascades is their stability. One expects that above a certain temperature the clusters will dissolve, whereas below this temperature they remain fixed. Such an effect may explain the following observed temperature dependence of D_{rad}. Below $\sim$ 150°C the cascades may not dissolve, and the AFS may be favored. As the temperature increases, more and more cascades may dissolve, and the conditions may change slowly into the MR region. This region is intermediate between

MR and AFS. We note that, if these ideas are correct, the sinks will also exist below 55°C, and the calculated D_{rad} will decrease by a factor of $10^4 \times C_s^{1/2}$ [eqn. (5)] below the values shown in Fig. 3.

We remark again that experiments to determine the actual defect structures as a function of time and temperature by both TEM and channeling techniques are under way, and they should replace the above speculative arguments.

4.4 Steady State

The model is based on the assumption that the concentration of vacancies and interstitials have attained steady state. The time to attain steady state, τ, is determined by the diffusion of the slow diffusing species (vacancies) to sinks[4]

$$\tau \approx 1/2\ K_{sv}\ C_s \qquad (6)$$

Values of τ calculated on the assumption that only grown-in dislocations act as sinks ($C_s = 10^{-8}$) are given in Table I. If collision cascades act as sinks, steady state will be reached more quickly as the sink density is higher, unless the sink density changes during the entire bombardment. In the latter case, steady state is not attained.

4.5 "Wind" Effects

Diffusion to the surface of point defects produced in the interior of the sample creates vacancy and interstitial winds.[27] The vacancy wind would enhance diffusion, and the interstitial wind would decrease diffusion. Calculations show that the flux due to the vacancy wind is about one-half

the diffusional flux and that the vacancy and interstitial winds should cancel each other to first order.[28] Interstitials formed deep within the sample may also affect the measured D_{rad}. The J vs x curve peaks at the end of the proton range ($\sim$ 1 μm from the surface), which is less than $\sqrt{D_i t}$ but much greater than $\sqrt{D_v t}$. Thus one expects excess interstitials to arrive in the diffusion zone; however, their numbers are difficult to calculate.

4.6 Comparison with Previous Work

The present results are qualitatively similar to those of Ermert et al. on diffusion in gold under α-particle irradiation.[15] In both cases, single crystals were used, so one expects to be in the MR region, yet D_{rad} is independent of T, and a factor of two drop occurs near the stage-IV temperature ($\sim$ room temperature). However, although our defect-production rate is $\sim$ 100 times that of Ermert et al., our D_{rad} is four times less than theirs.

The present results are rather different from those of Bystrov et al.,[14] which were obtained on Ag-8.75% Zn alloys under electron irradiation. They obtained an activation energy of 0.41 eV. However, their samples were so well annealed that steady state was not attained.

The study of Acker et al.[17] on the diffusion of Au and Cu in Al under neutron irradiation was carried out at much higher homologous temperatures than our work, and hence it can be assumed that their experiments attained steady state. The temperature dependence of their D_{rad} corresponds to MR dominant; however, the magnitudes of their measured D_{rad} are much larger than expected, unless the interstitials make a large contribution.

5. CONCLUSION

We have found that proton irradiation greatly enhances self-diffusion in silver. The results appear to agree qualitatively with the theory based on a two-defect model. Before final conclusions can be made, the density and structure of radiation-induced defect aggregates in the samples must be specified.

ACKNOWLEDGMENTS

We thank Prof. R. Sizmann for useful discussions, Dr. J. V. Sharp for permission to quote from his unpublished report, and Dr. J. R. Manning for discussion of the wind effect.

REFERENCES

1. See, for example, articles in *Radiation-Induced Voids in Metals*, J. W. Corbett and L. C. Ianello (eds) USAEC, 1972.
2. See, for example, R. L. Minnear, D. G. Nelson, and J. F. Gibbons, *J. Appl. Phys.* 43 (1972) 3468.
3. See, for example, the section on radiation damage in *High Voltage Electron Microscopy*, P. R. Swann, C. J. Humphreys, and M. J. Goringe, (eds). Academic Press, New York, 1974.
4. W. M. Lomer, UKAEA Report, AERE-T/R-1540, 1954 (unpublished).
5. G. J. Dienes and A. C. Damask, *J. Appl. Phys.* 29 (1958) 1713.
6. J. V. Sharp, UKAEA Report AERE-R-6267, 1969 (unpublished).
7. A. J. E. Foreman, *Rad. Effects* 14 (1972) 175.
8. S. J. Rothman, Nghi Q. Lam, R. Sizmann, and H. Bisswanger, *Rad. Effects* 20 (1973) 223.
9. Nghi Q. Lam, S. J. Rothman, and R. Sizmann, *Rad. Effects* (in press). We have, in the present paper, changed our notation for defect concentrations, etc., to conform to general usage in the field of radiation damage.
10. T. R. Waite, *Phys. Rev.* 107 (1957) 463.
11. L. N. Bystrov, L. I. Ivanov, and Yu. M. Platov, *phys. stat. sol. (a)* 8 (1972) 375.
12. We cite work on metals and alloys only. For work up to 1966, see the article by A. C. Damask, in *Studies in Radiation Effects on Solids*, G. J. Dienes (ed.) Gordon and Breach, New York, 1967, vol. 2, p. 1.
13. D. Heitkamp, W. Biermann, and T. S. Lundy, *Acta Met.* 14 (1966) 1201.
14. L. N. Bystrov, L. I. Ivanov, and Y. M. Platov, *phys. stat. sol. (a)* 7 (1971) 617.

15. U. Ermert, W. Rupp, and R. Sizmann, Int. Conf. on Vacancies and Interstitials in Metals (Jülich, Germany), vol. 2, p. 30 (1968).

16. D. Frenzel, *Z. Phys. Chem. (NF)* 51 (1966) 67.

17. D. Acker, M. Beyeler, G. Brebec, M. Bendazzoli, and J. Gilbert, *J. Nucl. Mater.* 50 (1974) 281.

18. G. Moreau, J. A. Cornet, and D. Calais, *J. Nucl. Mater.* 38 (1971) 197.

19. Nghi Q. Lam, S. J. Rothman, and L. J. Nowicki, *J. Electrochem. Soc.* 119 (1972) 715.

20. Nghi Q. Lam, S. J. Rothman, H. Mehrer, and L. J. Nowicki, *phys. stat. sol. (b)* 57 (1973) 225.

21. Nghi Q. Lam, S. J. Rothman, and K. L. Merkle, to be published.

22. O. G. Sutton, *Micrometeorology*, McGraw-Hill, New York, 1953, p. 216.

23. H. Mehrer and A. Seeger, *phys. stat. sol.* 39 (1970) 647.

24. See, for example, M. W. Thompson, *Defects and Radiation Damage in Metals*, Cambridge, 1969, Ch. 4 and 5.

25. P. G. Lucasson and R. M. Walker, *Phys. Rev.* 127 (1962) 485.

26. K. L. Merkle, P. P. Pronko, D. S. Gemmell, R. C. Mikkelson, and J. R. Wrobel, *Phys. Rev. B* 8 (1973) 1002.

27. J. R. Manning, *Diffusion Kinetics for Atoms in Crystals*, Van Nostrand, Princeton, N. J., 1968, Ch. 4

28. J. R. Manning, National Bureau of Standards, private communication, 1974.

FIGURE CAPTIONS

Fig. 1. Penetration plots for radiation-enhanced diffusion in silver single crystals at high temperatures, $J = 6.5 \times 10^{-6}$/sec.

Fig. 2. Penetration plots for radiation-enhanced diffusion in silver single crystals for low temperatures, $J = 6.5 \times 10^{-6}$/sec.

Fig. 3. Temperature dependence of the proton radiation-enhanced diffusion coefficient D_{rad} for silver. The dashed line for diffusion without irradiation is from Ref. 20. The theoretical lines are calculated from eqns. (2) and (5).

Fig. 4. Flux dependence of D_{rad} for silver bombarded with 270-keV protons at T = 106°C.

Fig. 5. Flux dependence of D_{rad} for silver bombarded with 270-keV protons at T = 179°C.

TABLE CAPTIONS

Table I Temperature Dependence of D_{rad} Calculated for the Maximum and Minimum Defect-production Rates.

Table II Flux Dependence of D_{rad} at T = 106°C.

Table III Flux Dependence of D_{rad} at T = 179°C.

Table I. Temperature Dependence of D_{rad} Calculated for the Maximum and Minimum Defect-production Rates

Temperature (°C)	Irradiation Time (10^4 sec)	D_x (10^{-11} cm/sec)	D_{rad} (10^{-17} cm^2/sec) ($J = 6.5 \times 10^{-6}$/sec) (Max. calculated J)	D_{rad} (10^{-17} cm^2/sec) ($J = 8.5 \times 10^{-7}$/sec) (Min. calculated J)	τ calculated from eqn. (6) (sec)
- 59.7	3.85		1.54		4.1×10^{13}
- 20.0	3.00		1.77		3.1×10^{11}
- 1.9	2.88		3.92		2.4×10^{9}
23.4	2.55		3.96		1.1×10^{8}
23.4	4.32		2.81		1.1×10^{8}
55.5	2.28		5.05		4.5×10^{6}
83.8	1.80	2.55	5.02	38.5	4.3×10^{5}
106.0	2.16	2.65	5.40	41.5	8.7×10^{4}
131.6	2.52	2.87	6.32	48.6	1.7×10^{4}
159.8	1.83	2.76	5.86	45.0	3.6×10^{3}
159.8	2.16	2.26	3.93	30.2	3.6×10^{3}
159.8	2.43	2.74	5.77	44.4	3.6×10^{3}
178.8	1.98	2.89	6.42	49.3	1.4×10^{3}
213.0	2.16	3.37	8.74	67.2	3.0×10^{2}
213.0	0.99	3.87	11.52	88.6	3.0×10^{2}
240.6	2.16	3.85	11.39	87.6	1.0×10^{2}

Table II. Flux Dependence of D_{rad} at T = 106°C

Flux (10^{13} protons/cm^2-sec)	Irradiation Time (10^4 sec)	D_x (10^{-11} cm/sec)	J (10^{-6}/sec)	D_{rad} (10^{-17} cm^2/sec)
0.313	3.20	1.02	1.6	3.23
1.25	2.16	2.65	6.5	5.40
3.13	0.75	4.61	16.0	6.50
6.25	0.48	12.70	32.0	24.70

Table III. Flux Dependence of D_{rad} at T = 179°C

Flux (10^{13} protons/cm^2-sec)	Irradiation Time (10^4 sec)	D_x (10^{-11} cm/sec)	J (10^{-6}/sec)	D_{rad} (10^{-17} cm^2/sec)
0.25	2.88	0.826	1.3	2.63
1.25	1.98	2.89	6.5	6.42
2.50	1.32	4.91	13.0	9.28
6.25	0.57	8.61	32.0	11.50

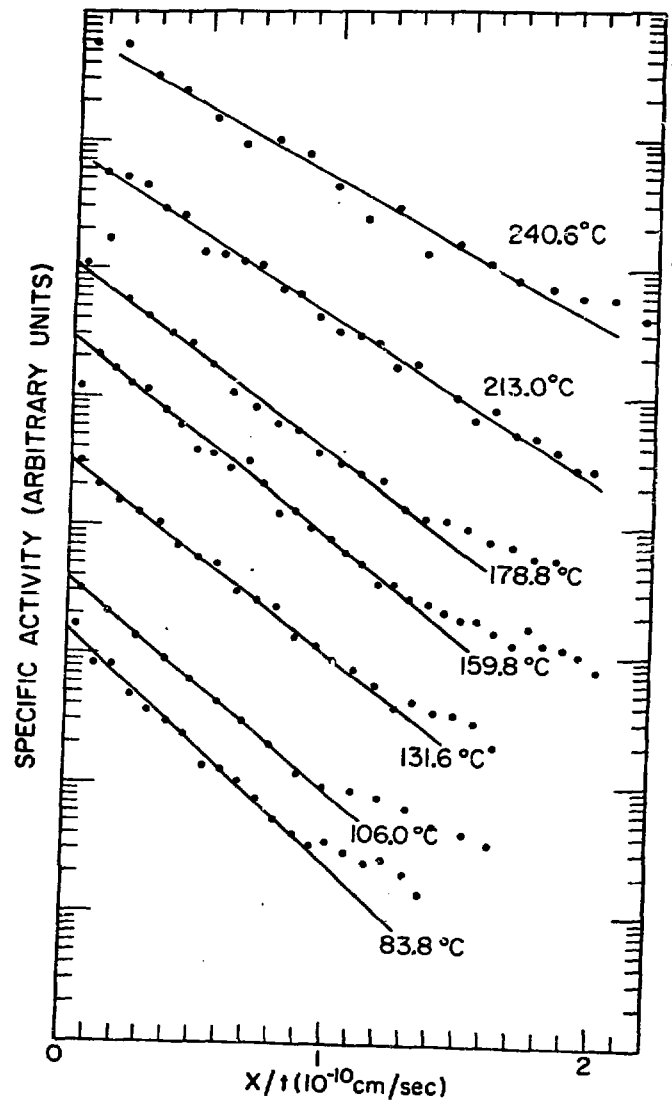

Fig. 1. Penetration plots for radiation-enhanced diffusion in silver single crystals at high temperatures, J = 6.5 x 10^{-6}/sec. Neg. No. MSD-60145

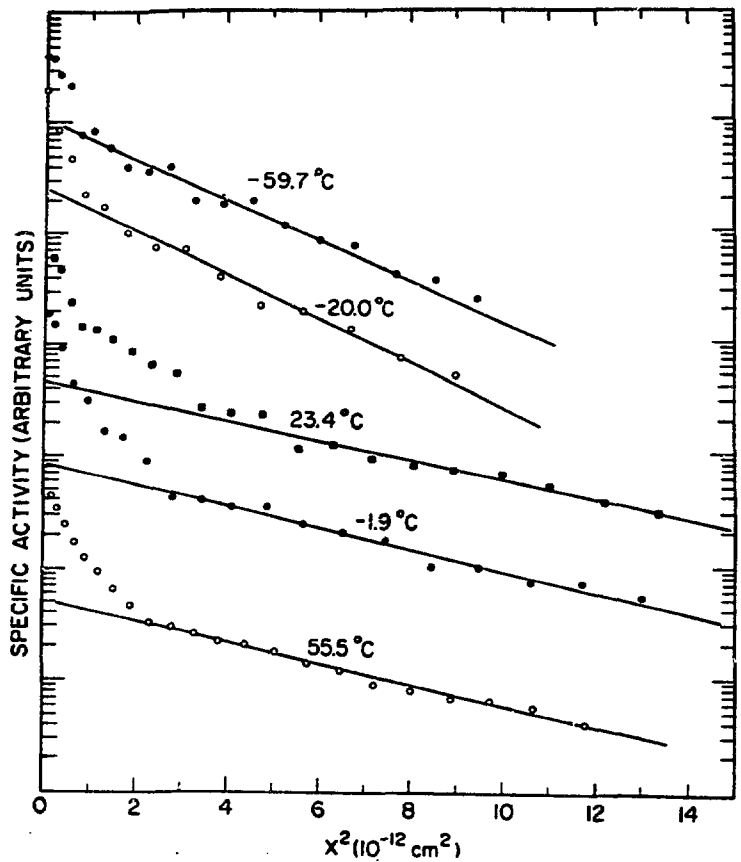

Fig. 2. Penetration plots for radiation-enhanced diffusion in silver single crystals for low temperatures, $J = 6.5 \times 10^{-6}$/sec. Neg. No. MSD-60146

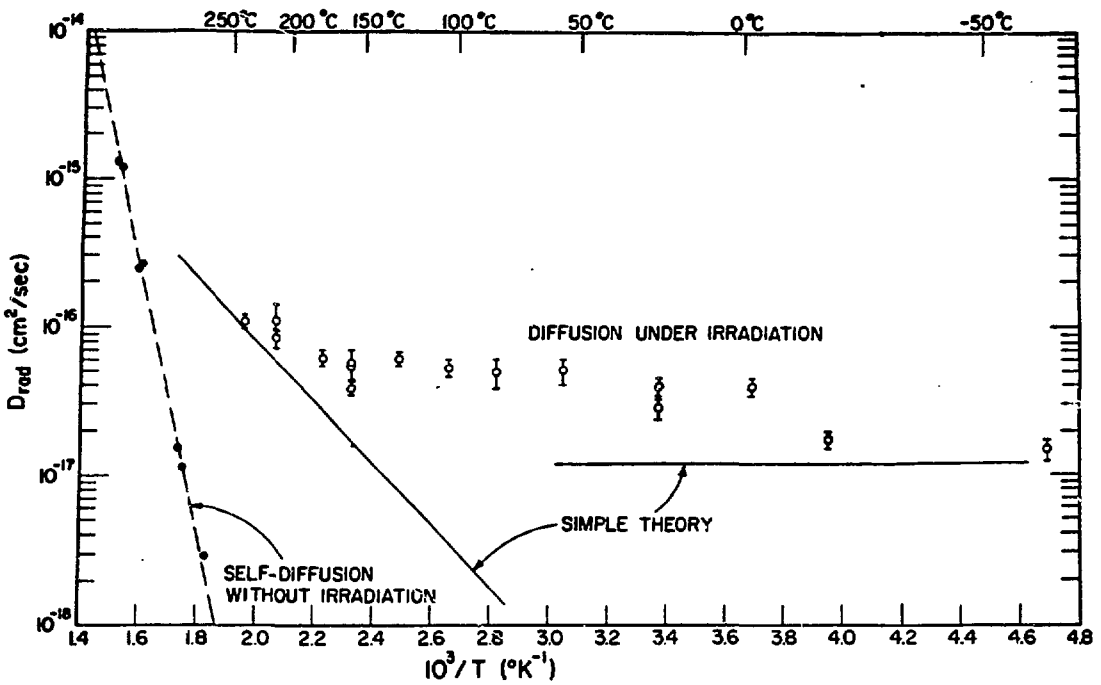

Fig. 3. Temperature dependence of the proton radiation-enhanced diffusion coefficient D_{rad} for silver. The dashed line for diffusion without irradiation is from Ref. 20. The theoretical lines are calculated from eqns. (2) and (5). Neg. No. MSD-60147

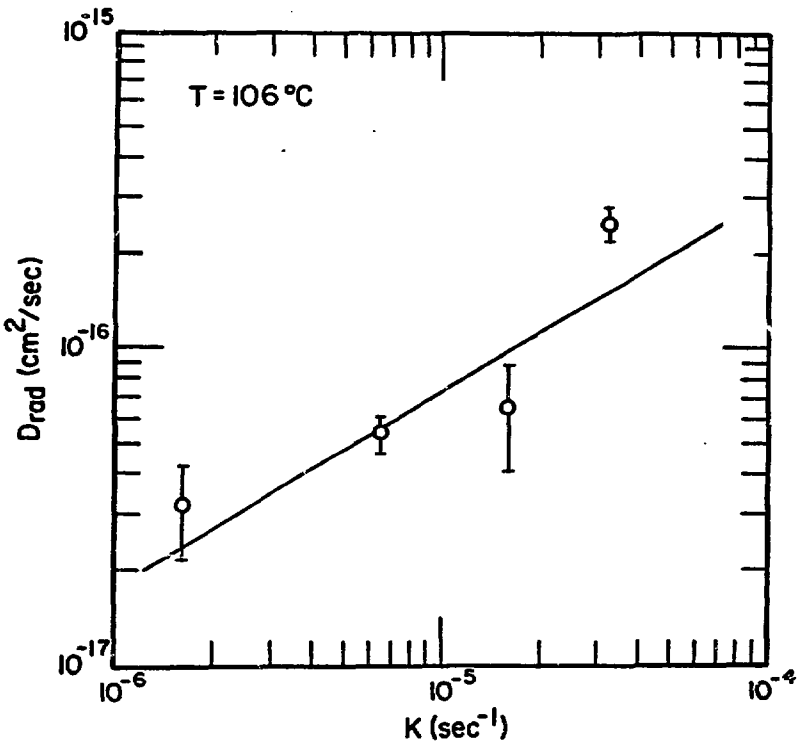

Fig. 4. Flux dependence of D_{rad} for silver bombarded with 270-keV protons at T = 106°C. Neg. No. MSD-60143

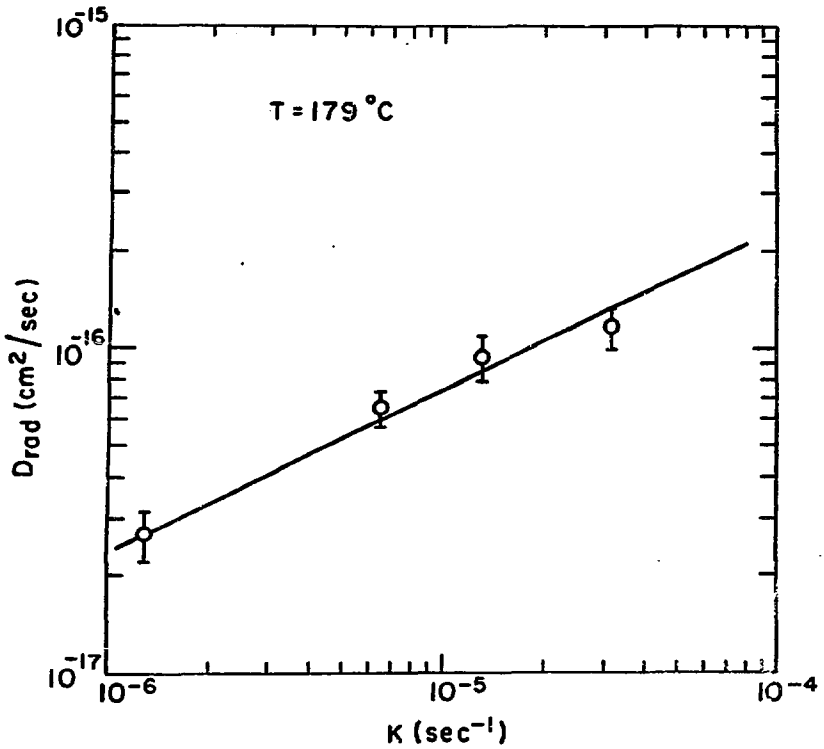

Fig. 5. Flux dependence of D_{rad} for silver bombarded with 270-keV protons at T = 179°C. Neg. No. MSD-60144.